PCCP

Accepted Manuscript

ROYAL SOCIETY OF CHEMISTRY

www.rsc.org/pccp

Journal Name

ARTICLE TYPE

Cite this: DOI: 10.1039/xxxxxxxxxx

Role of Ligand-Ligand vs. Core-Core Interactions in Gold Nanoclusters†

Karolina Z. Milowska,*‡ and Jacek K. Stolarczyk,*

Received Date
Accepted Date

DOI: 10.1039/xxxxxxxxxx

www.rsc.org/journalname

The controlled assembly of ligand-coated gold nanoclusters (NCs) into larger structures paves the way for new applications ranging from electronics to nanomedicine. Here, we demonstrate through rigorous density functional theory (DFT) calculations employing novel functionals accounting for van der Waals forces that the ligand - ligand interactions determine whether stable assemblies can be formed. The study of NCs with different core sizes, symmetry forms, ligand lengths, mutual crystal orientations, and in the presence of a solvent suggests that core-to-core van der Waals interactions play a lesser role in the assembly. The dominant interactions originate from combination of steric effects, augmented by ligand bundling on NC facets, and related to them changes in electronic properties induced by neighbouring NCs. We also show that, in contrast to standard colloidal theory approach, DFT correctly reproduces the surprising experimental trends in the strength of the inter-particle interaction observed when varying the length of the ligands. The results underpin the importance of understanding NC interactions in designing gold NCs for a specific function.

1 Introduction

Gold nanoclusters (AuNCs) of sizes up to few nanometers exhibit distinctive properties unseen in their larger counterparts or in the bulk.[1–3] For instance, they do not support plasmon resonance, but undergo electronic transitions with non-zero band gap.[3] Due to unique quantum confinement effects and geometric constraints their optical, electronic and catalytic properties are strongly dependent on the number of constituent atoms and as well as on the type, number and length of the coordinating ligands. The ability to precisely tune the properties by varying the synthetic approach holds promise for applications in light harvesting[4], light emitting[5], electronic devices[6], and catalysis[7,8].

Assembly of thiol-protected AuNCs into 2D[9] and 3D[10,11] arrays and supraparticles opens a pathway to attain additional functionalities which stem from the collective features of the ordered nanocrystals[12]. The applicability of a specific structure, e.g. as a sensor[6], relies on the arrangement of the AuNCs and on the interparticle distances within the structure. These parameters determine the light absorption, interparticle charge transfer[13] and other relevant properties. In this context, it is clear that understanding of the interactions governing the self-assembly of the nanocrystals is prerequisite for controlling the assembly process itself as well as the emergent properties of the resulting 3D superstructure[14,15]. Despite significant progress in the field in recent years, it is still subject to much debate as to which interaction plays a dominant role in the assembly.

The interactions of the alkanethiol ligands with the corresponding ligands of the neighboring particle[16,17] or, if present, with the solvent molecules[18] are often considered to govern the assembly. The interdigitation of the soft ligand chains is considered as an important factor determining the separation of the particles[19]. For small non-spherical AuNCs the interdigitation is found to be sensitive to the distribution of the ligands on the nanocrystal facets. Interestingly, the effect of the faceting on the separation and particle arrangement can be pronounced even for long-chain ligands[10]. Nonetheless, the tendency of the AuNCs to form an ordered structure decreases with the increase of the length of the ligand[20]. On the other hand, experiments supported by simulations[18,21] suggests that, especially for larger NCs, van der Waals attraction of the cores and their geometry should significantly affect the nucleation of a superstructure and help determine the eventual arrangement of the NCs[22,23], leaving the original question unresolved.

Two approaches have been predominantly used to calculate the

Photonics and Optoelectronics Group, Department of Physics and Center for NanoScience (CeNS), Ludwig-Maximilians-Universität München, Amalienstr. 54, 80799 Munich, Germany. Fax: +49 89 2180 3441
Nanosystems Initiative Munich (NIM), Schellingstr. 4, 80799 Munich, Germany.
E-mail: kzm21@cam.ac.uk
E-mail: Jacek.Stolarczyk@physik.uni-muenchen.de
† Electronic Supplementary Information (ESI) available: [details of any supplementary information available should be included here]. See DOI: 10.1039/b000000x/
‡ Present address: Department of Materials Science and Metallurgy, University of Cambridge, 27 Charles Babbage Rd, Cambridge CB3 0FS, United Kingdom

nanoparticle interactions, depending on the scale of the investigated objects. The framework of colloidal stability theory (CST), developed initially for particles with sizes exceeding 100nm[24,25], was successfully applied to much smaller nanoparticles, even less than 10nm in diameter[15,26–28]. The theory assumes contributions to the interaction potential from van der Waals, steric, electrostatic, and magnetic forces, where the latter two are not needed for thiolated AuNCs. The evaluation of these interactions is fairly straightforward for spherical nanoparticles and other simple geometries[15,29]. However, for the ultra-small nanoparticles, where the range of interactions is comparable to the local radius of curvature and the faceted nature of the nanocrystal surface starts to manifest itself, the assumptions made in the development of the theory no longer hold. Therefore for particles smaller than about 5nm, the accuracy of such calculations is expected to be significantly worse[30]. On the other hand, density functional theory (DFT) calculations made it possible to accurately determine the structure and predict properties of NCs[2,3,31]. However, due to computational constraints, it is only practically applicable to particles of diameter less than 2 nm. In this context, the middle ground between the colloidal and the molecular (*ab initio*) applicability regimes, which is occupied by few-nanometer-sized nanocrystals, does not appear to be effectively described by either of the two approaches. Clearly, more theoretical studies are needed to understand the interactions and assembly of such particles.

Accordingly, in this paper, we have applied both approaches, DFT and CST, to calculate the interaction potentials between AuNCs of several different sizes up to Au_{144} and protected with alkanethiol ligands of different length (-S(C_nH_{2n+1}), n=1,..,8). As the properties of the AuNCs vary significantly with their size and shape, we have firstly used DFT to rigorously determine the structure of nine thiolated NCs (Au_{11}, Au_{13}, Au_{16}, Au_{19}, Au_{38}, Au_{55}, Au_{79}, Au_{102} and Au_{144}). To this end, we have employed two novel exchange-correlation functionals accounting for the van der Waals force. Subsequently, we have compared the theoretical interaction potentials with the available experimental data in order to evaluate the driving force of the self-assembly of AuNCs. We have found the dominant role of the ligand-ligand interactions, which originate from combination of steric interactions of AuNCs caused by non-uniform distribution of the ligands on the surface and related to them changes in electronic properties induced by vicinity of a second NC. These aspects of the AuNCs interactions are poorly reproduced by the colloidal calculations.

2 Methodology

2.1 *Ab initio* approach

The calculations have been carried out in the framework of the spin polarized DFT[32,33] realized in the SIESTA numerical package[34,35]. Generalized gradient approximation (GGA) of the exchange-correlation functional in Perdew-Burke-Ernzerhof (PBE)[36] parametrization has been applied to all systems. For the smallest considered system, Au_{11}, also local density approximation (LDA) of the exchange-correlation functional in Ceperley-Alder (CA)[37] parametrization and non-local van der Waals functionals (VDW)[38,39] have been used. Valence electrons have been represented with double zeta numerical basis sets of orbitals localized on atoms including polarization functions. The influence of core electrons has been accounted within the pseudopotential formalism. Norm-conserving Troullier-Martins nonlocal pseudopotentials[40] have been cast into the Kleinman-Bylander separable form.[41] The kinetic cut-off for real-space integrals has been set to 350 Ry (450 Ry for VDW). The Brillouin zone has been sampled in the 1x1x1 Monkhorst and Pack scheme.[42] In other words, only the Γ point of the supercell was used in all calculations. During all calculations, the self-consistent field (SCF) cycle has been iterated until the total energy changed by less than 10^{-5} eV/atom. The density matrix convergence criterion has been set to 10^{-5}. The maximum force tolerance equaled 0.01 eV/Å.

To obtain structure of all studied types of AuNCs the calculations have been performed within the supercell scheme. The AuNCs have been separated by a distance large enough to eliminate any interaction and their structure has been optimized to get vanishingly small forces on atoms (i.e. the size of the supercell for Au_{38} protected by -SCH_3 ligands was: 35x35x35 $Å^3$). We have used the binding energy per atom as the measure of the stability of the studied systems. Since synthesis of thiol-derivated gold nanoparticles is done by simultaneous attachment of ligands to the core with growth of core[43,44], the usage of binding energy instead of adsorption energy (heat of formation) seems to be more appropriate. Hence, the binding energy per atom has been calculated according to the formula:

$$E_{bind/N_\alpha} = \frac{1}{N_\alpha}\left(E_{system} - \sum_{\alpha=1}^{N_\alpha} E_{atom,\alpha}\right), \qquad (1)$$

where N_α is the number of atoms in the system, and $E_{atom,\alpha}$ is the total atomic energy of the free atom of type α (C, S, Au or H).

Our DFT calculations are based on the ground state total energy calculations, which do not include vibrational dynamical contribution to the free energy. Therefore, in order to optimize the geometries of all systems, we have performed very rigorous search through the configurational space. This procedure guarantees obtaining the energetically most favourable configurations. Comparing morphology and stability of all structures we always refer to systems characterized by equilibrium geometry.

In next step the interaction potentials have been calculated. Therefore, inside supercell two chosen NCs have been placed and the distance between them has been changed to obtain curve. The relative energy of interations as a function of distance r between AuNCs can be described as:

$$\begin{aligned} E_{rel} &= E_{total}^{2AuNC}(r) - 2\cdot E_{total}^{AuNC}(\infty) + E_{corr}, \\ E_{corr} &= E_{total}^{AuNC+ghost}(r) - E_{total}^{AuNC}(\infty) + \\ &+ E_{total}^{ghost+AuNC}(r) - E_{total}^{AuNC}(\infty), \end{aligned} \qquad (2)$$

where $E_{total}^{2AuNC}(r)$ and $E_{total}^{AuNC}(\infty)$ are the total energies of the two AuNCs at distance r and an isolated NC. E_{corr} is basis set superposition error correction (BSSE) due to usage of the numerical code with a localized basis.[45–47] $E_{total}^{AuNC+ghost}(r)$ and $E_{total}^{ghost+AuNC}(r)$ are

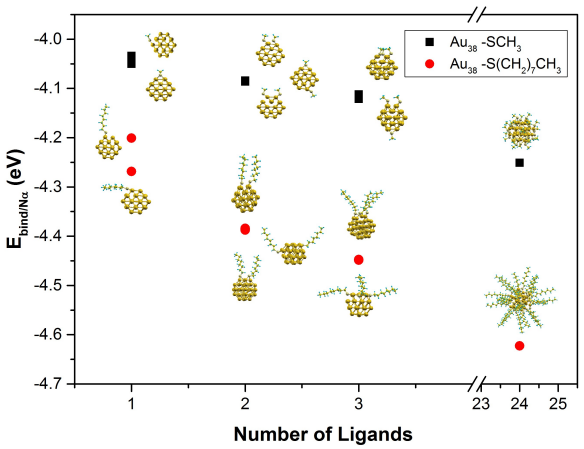

Fig. 1 Binding energy per atom for different binding scenarios of the methylthiol (-SCH_3) and octylthiol (-SC_8H_{17}) ligands to the surface atoms (facets) of the Au_{38} NC, together with optimized structures.

Kohn-Sham energies of the two NCs system where one of the NCs is replaced by their ghosts[35] and all atoms are fixed on optimized positions at chosen distance r.

2.2 Colloidal approach

The colloidal model assumes that the contributions from each individual interaction are additive, so that the total interaction potential can be expressed as their sum:

$$\Phi = \Phi_{vdW} + \Phi_{steric}, \quad (3)$$

where Φ_{vdW} is the van der Waals attraction between the nanoparticles, and Φ_{steric} describes steric interactions. In general all the interactions can be either attractive or repulsive, becoming a driving force for aggregation or preserving stabilization of system, depending on the specific conditions. However, in vast majority of cases the van der Waals component is negative, i.e. attractive, whereas the steric component is almost always repulsive. The details of this model with all necessary parameters are provided in the ESI.

3 Results and discussion

3.1 Nanocluster formation

According to the experimental observations[48] and previous theoretical investigations[49] AuNCs appear mostly in cube-octahedra, truncated octahedra and icosahedral symmetry forms. We have started our investigation with set of nine AuNCs covering the relevant range of sizes and representing the different core symmetries. The initial core structures were taken from literature among most often reported. Specifically, Au_{11} has cyclic symmetry[50]. Five of chosen NCs, Au_{13}, Au_{19}, Au_{38}, Au_{55}, and Au_{79} have octahedral symmetry[49]. Au_{16} has tetragonal symmetry[49], whereas Au_{102} has pentagonal decahedral symmetry[51]. Finally, Au_{144} has been chosen as representative of icosahedral symmetry[52,53]. The growth of gold core occurs at the same time as attachment of ligands to the core[43,44]. In order to understand the synthesis route of thiolated AuNCs and their morphology, we have built the Au core of predefined size as spherical cut from face-centered cubic Au bulk[49], such that the above listed symmetries are fulfilled. In the next step, we added ligands and then fully optimized the whole system.

Table 1 Parameters characterizing morphology of thiolated gold ultra-small nanoparticles: Au-Au_s - the average bond lengths between Au atoms on core surface, Au-Au_c - the average bond lengths between Au atoms inside the core, and Au-S - the average bond lengths between Au and S, as calculated with standard exchange-correlation functionals (GGA and LDA) and two describing van der Waals interactions (VV and KBM). Experimental values describe structures of 3 nm tiopronin-capped Au nanoparticles (I) and Au_{102} AuNCs protected with p-mercaptobenzoic acid (II).

	Au-Au_s (Å)	Au-Au_c (Å)	Au-S (Å)
DFT, GGA (PBE)	2.86	2.88	2.43
DFT, LDA (CA)	2.81	2.87	2.40
DFT, VDW (VV)	2.86	2.90	2.43
DFT, VDW (KBM)	2.88	2.88	2.41
Experiment I[54]	2.85	2.85	2.46
Experiment II[51,55]	—	2.8-3.1	2.2-2.6

The structural properties of protected AuNCs have been studied in DFT approach. The DFT relies on various approximations to the exchange and correlation functionals that are nowadays prerequisites for practical implementations of DFT. In spite of a long list of successes, commonly used LDA and GGA, both possess some significant drawbacks. One of them is rather poor description of van der Waals interactions. Therefore, in the first-principle calculations performed in DFT framework we have implemented novel functionals accounting for van der Waals forces to structural analysis of thiolated AuNCs. The results of calculations employing standard functionals (CA, PBE) and functionals designed to describe van der Waals interactions (Vydrov-Voorhis (VV)[38], Klimes-Bowler-Michaelides (KBM)[39]) are summarized and compared to the experimental findings in Tab. 1.

LDA describes fairly well Au-Au bond lengths inside the NC core and underestimates Au-S bond lengths due to well known over-binding problem. GGA overestimates Au-Au bonds inside the core, whereas Au-S are quite close to the experimental values. Both employed van der Waals functionals give Au-Au bond lengths very close to the experimental values. VV better describes Au-S bond lengths than KBM, therefore we have chosen VV for further study. However, due to computational cost of using VDW functionals, GGA functional is also a reliable choice. Our structural parameters are very close to those obtained with hybrid potentials (BLYP)[56,57] and post Hartree-Fock methods[57].

Ligands and their distribution over a core play a key role for NC functionality. As shown in Fig. 1, the system becomes, as expected, more stable with adding more ligands. The chosen test case of Au_{38} NC has two types of crystal facets, namely (100) and (111). It transpires that the ligands preferentially bind to (100) facet rather than (111). Binding the second ligand to the same (100) facet is more probable than to the different (100) facet or (111) facet. However, the second ligand will be attached as far as possible from the first one to the same facet. The energetic differences between those configurations are rather small (less

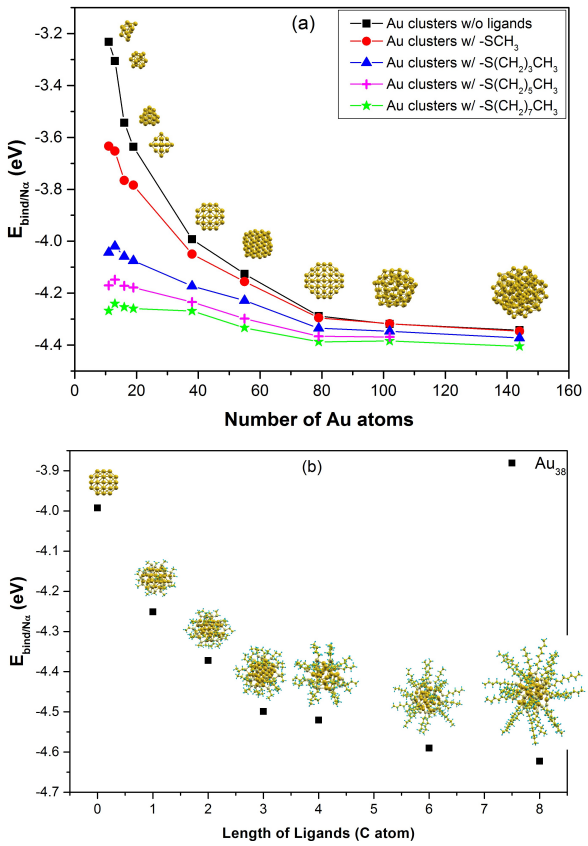

Fig. 2 (a) Binding energy per atom as function of a number of Au atoms in the NC and the length of one ligand. (b) Binding energy per atom for multiple ligands providing maximal coverage of Au_{38} NC as a function of the length of the ligand.

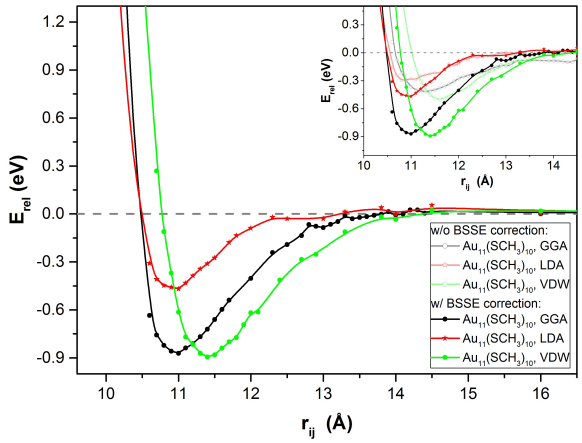

Fig. 3 Interaction potential profile vs centre-to-centre separation for two Au_{11} NCs, calculated using different functionals: GGA, LDA, and VDW in VV implementation. Inset: Results obtained without BSSE correction are marked with open symbols, whereas closed symbols indicate corrected relative energy.

than 0.0002 eV for $-SCH_3$ and less than 0.0026 eV for $-SC_8H_{17}$). Arrangement of ligands depends on the type of facet leading to differences in packing density of thiols on core surface. In other words, ligands create bundles on core surface. Interesting consequence was observed recently by Goubet and Pileni[58]. The formation of negative gold supracrystals was explained through presence of concentrated zones of alkyl thiolates on core surface due to well pronounced crystal facets.

Thiolated gold cores become corrugated by binding of ligands. The bond between S and Au has a strong covalent character, comparable with Au-Au bond. Therefore, especially for smaller cores like Au_{11}, the initial symmetry is significantly disturbed. Amorphization process leads to strain relief and in consequence to energy minimization. Our findings are in good agreement with experimental data. Mariscal et al.[59], who studied atomic structure of passivated gold nanoparticles smaller than 2 nm reported that crystalline structure of cores is highly altered. Jadzinsky et al.[51] were able to obtain a clear picture of linear RS-Au-RS bindings motifs present on the core surface, which they called 'staple' motifs. Jiang et al.[60] showed that once created 'staple' motifs do not dissociate and help to preserve nanoparticle geometry. We have found out that binding of two separate bridges on one (100) facet of Au_{38} is more probable than binding all together all four Au atoms by S atoms. The energy difference is equal 0.021 eV. Square bridge geometry is preferred when the number of thiol groups increases. Such gold-thiolate tetraunits were also observed by Häkkinen et al.[61] The characteristic alignment of ligands on certain crystal facets was found not only on AuNCs[62], but also on PbS or CdSe NCs[63].

The dependence of binding energy per atom on number of attached ligands is a non-linear function. The binding energy of Au_{38} with one $-SCH_3$ ligand is equal to -4.05 eV, with two ligands -4.09 eV, with 3 ligands -4.12 eV, with 10 ligands -4.22 eV and with 24 ligands -4.25 eV. It is clear that the decrease of magnitude of binding energy per atom is more pronounced for low ligand concentrations, in agreement with earlier observations[60,64]. The number of ligands and therefore the coverage of each NC is well defined. This is why, it is possible[65] to control the gold particle size by changing the Au/alkanethiol molar ratios.

Next, we have studied the effect of the core size and the length of the ligands protecting AuNCs (see Fig. 2). Larger NCs, containing smaller proportion of the surface atoms, are more stable, as expected. In agreement with experiment[66], longer ligands are preferred for the stability of NC. Similar results were obtained when only one ligand molecule was used (Fig. 2 (a)) as well as with full coverage of the core surface by the alkanethiol ligands (Fig. 2 (b)).

3.2 Nanocluster interactions

Through careful synthesis and sample preparation it is possible to obtain modisperse AuNCs of selected size.[67–69]. Therefore, we focus here only on the interactions between identical NCs. Among nine considered NCs we have chosen for further study the smallest one, Au_{11}, the biggest one, Au_{144}, and Au_{38} which has two different types of crystal facets. These three representatives cover the relevant and computationally accessible range of NC sizes. We have placed two chosen optimized NCs inside a supercell and varied the distance between them to obtain an energy profile. The structures of NCs have not been optimized after the placement.

Let us start with comparison of standard exchange-correlation functionals (PBE, CA) with non-local van der Waals functional (VV). The interaction potential profiles for two $Au_{11}(SCH_3)_{10}$ NCs calculated using these functionals are plotted in Fig. 3. The positions of minimum and the depth of potential curves differ slightly due to different values of bond lengths obtained in those three approaches.

We have also analyzed the impact of BSSE correction on interaction potential profiles. The BSSE corrections are much more important in systems that the interaction occurs via physical regime than by chemical bond and cannot be neglected here.[46,47,64,70] In order to verify that fact we have compared interaction potential before and after BSSE correction (see inset in Fig. 3). The interaction potentials are not only shifted to more negative values (become more attractive), but also position of minimum and shape of potential curve itself is altered. As expected, BSSE correction is necessary in those systems. The deepest minimum can be observed for van der Waals functional, whereas local density approximation gives the shallowest minimum. Surprisingly, after BSSE correction the distance between van der Waals and general gradient approximation decreases significantly. This confirms our decision to use GGA rather than VDW functional in further calculations. The position of minimum for VDW is shifted about 0.4 Å in comparison to GGA and LDA. This is due to longer Au-Au bonds predicted by VDW approach.

We have also checked the influence of optimization on our results. The curve obtained by optimization in each step contains few minima and is not as smooth as the curve obtained without optimization in each step. Alteration of distance between AuNCs the system substantially changes its conformation especially, when two NCs are put closely together.

In the next step we have compared CST and DFT approaches. In Fig. 4 (a) and (b) the dependence of interaction potential on distance between centres of cores for different sizes of AuNCs according to DFT and CST is depicted. The DFT results do not present clear trend of clustering probability as a function of core size. The potential depth is significantly different for the smallest studied system, $Au_{11}(SCH_3)_{10}$, and almost thrice deeper than for $Au_{38}(SCH_3)_{24}$ NC. This is due to non-spherical shape and absence of defined facet of $Au_{11}(SCH_3)_{10}$ NC. Nevertheless, for bigger AuNCs, trend is in agreement with expectations based on experiments[21]: $Au_{38}(SCH_3)_{24}$ will create less stable assembly than $Au_{144}(SCH_3)_{60}$. This observation is in agreement with Monte Carlo (MC) and MD[71,72] simulations of bigger systems. Also previous[18] CST studies of bigger gold nanoparticles indicated that interaction peaks becomes more attractive with increasing nanocrystal size. The differences in relation between the smallest considered AuNCs, $Au_{11}(SCH_3)_{10}$, and $Au_{38}(SCH_3)_{24}$ in DFT and CST approaches result mainly from neglecting the NC shape in the colloidal approach.

The dependence of interaction potential between two AuNCs on ligand length is presented in Fig. 5. Potential well of protected AuNCs obtained in DFT approach are order of magnitude shallower than of bare cores (cf. inset in Fig. 5 (a)). This is as expected - the unprotected AuNCs tend to aggregate, especially in the absence of solvent. Their preparation, conservation and protection require passivation with ligand molecules[59].

Generally, the depth and position of interaction potential is different for different length of ligands in DFT approach. The interaction potentials of $Au_{38}(SC_2H_5)_{24}$ and $Au_{38}(SC_3H_7)_{24}$ differ from the rest of considered systems (see Fig.S1 in ESI). This effect for small ligands is well known problem of simulations that do not contain solvent[49,61]. Ligands in those two cases are bent closely to core surface, which is also slightly altered from bare case. Starting from $-SC_4H_9$ ligand, the situation is changed - AuNCs are hedgehog-like structures, where ligand are sticking out from core surface in all directions and only their segments close to the core are tilted. Also, in MD simulation the 20-35^o tilting of alkyl chains with respect to the surface normal was observed[16,73,74]. The results presented in this section correspond to the equilibrium situation at 0 K. Besides the bending effect, we do not have any configurational defects in ligand chains. The results of experiments[19] indicate that below the calorimetrically-determined phase transition temperature the *gauche* defect density is low in the middle of the chain and near the sulfur head group. Moreover, the detectable amount of *gauche* defects decreases with increasing chain length.[75].

In experiments[10,21,76], longer ligands are used, such as hexane- and dodecanethiols. Therefore, it is better to compare only the interaction potential of $Au_{38}(SCH_3)_{24}$, $Au_{38}(SC_4H_9)_{24}$, and $Au_{38}(SC_6H_{13})_{24}$. The potential well deepens, therefore the clustering becomes more likely with increasing the length of the ligands. These intriguing DFT results are in good agreement with MC and MD predictions[71,72]. Moreover, our results correspond well with earlier experimental studies showing a pronounced role of faceting even for longer ligands[10]. The trend obtained in framework of CST is opposite. It shows that increase of ligand length leads to shallower well depth. The shapes of interaction potentials presented in Fig. 5 (a) are similar to each other, whereas in Fig. 5 (b) one can see that potential curve is broader with increasing lengths of ligand. The steric component of Φ_{tot} increases with increasing length of ligands, whereas van der Waals part remains the same. In colloidal approach, the vdW interactions are explicitly accounted only for the cores, but not for the ligands. Previous Brownian Dynamics simulations[18,77], in which nanoparticles interactions were described in CST approach, predicted interactions between bigger Au nanoparticles more attractive when the ligand film curvature is reduced.

The influence of solvent on interactions between two gold nanoparticles is considered[20,21,78,79] to be one of the most important factors for obtaining required type of supracrystals. To check the effect of solvent on AuNCs interactions in DFT approach, we have introduced toluene molecules into supercell with two $Au_{38}(SCH_3)_{24}$ (see Fig. 6). NCs, as well as solvent molecules have been fully optimized. The binding energy of system containing solvent molecules is slightly reduced in comparison to system without toluene. The energy difference is equal to 0.061 eV. This means, despite only a small difference in cohesion energy density of the solvent and ligand (as expressed by their Hildebrand parameters equal 18.2 and 15.5, respectively), the solvent molecules will be pushed out from the interparticle space and will allow for a closer approach of the NCs. The solvent exclusion

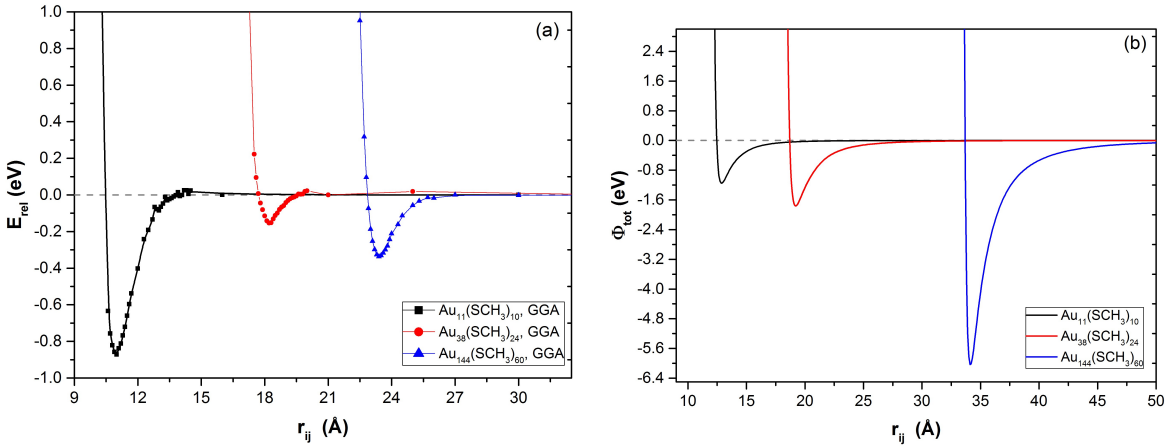

Fig. 4 Interaction potential profile calculated in (a) *ab initio* and (b) colloidal approach between two AuNCs for different size of the NC: $Au_{11}(SCH_3)_{10}$, $Au_{38}(SCH_3)_{24}$ and $Au_{144}(SCH_3)_{60}$. Distance r_{ij} is the distance between centers of cores.

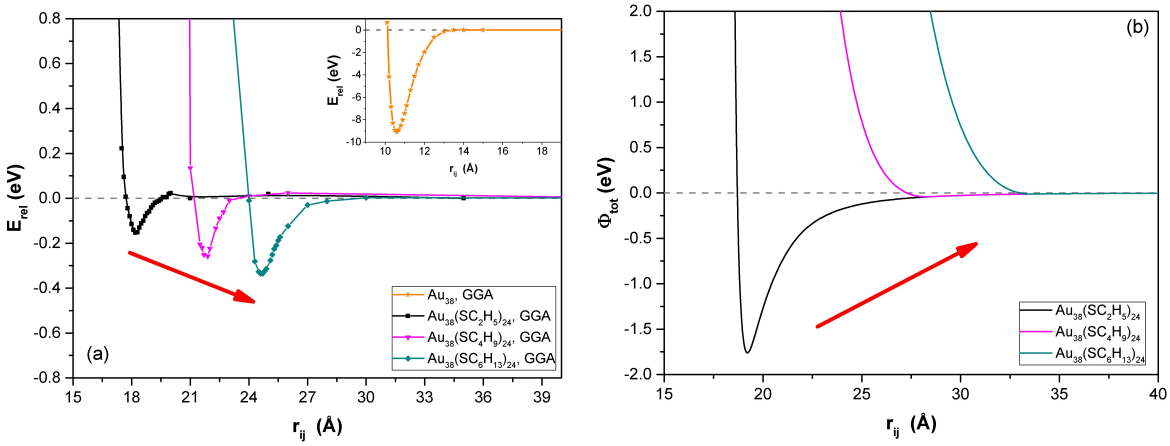

Fig. 5 Interaction potential profile calculated in (a) *ab initio* and (b) colloidal approach between two Au_{38} NCs for different length of the ligand. Distance r_{ij} is the distance between centres of cores. Trends are marked by red arrows.

likely stems from the mismatch between the available space between the ligands and molecular size of the solvent, demonstrating the need for non-continuum models to be used at this scale. The effect is indeed observed in experiments [18,80] and reported in MC study [73] of thiol passivated Au surface.

Since there is no consensus which interactions - between ligands or between cores are dominant, we have decided to study the influence of crystal orientation of interaction potential of AuNCs. For this purpose, we have chosen Au_{38} NCs with well-defined two crystal facets. Specifically, the relative interaction energy between two Au_{38} cores, two $Au_{38}(SCH_3)_{24}$ and two $Au_{38}(SC_4H_9)_{24}$ NC at a distance 25 Å as a function of angle between two different (100) facets has been determined. The positions of atoms in second AuNC are obtained by translation and clockwise rotation by angle around centre of mass of that AuNC (see Fig.S2). Cores in both AuNCs are frozen, whereas ligands have been optimized to get vanishingly small forces. The differences in relative energies for ten angles between 0^o and 45^o are: 0.088 eV, 0.019 eV and 0.093 eV for Au_{38}, $Au_{38}(SCH_3)_{24}$, and $Au_{38}(SC_4H_9)_{24}$, respectively. Adding ligands to the core works as an isolation layer to the core and difference in relative energies is reduced. However, for longer ligands the difference is not only increased in comparison to shorter ligands, but also to unprotected cores. It means that interactions between ligands start to play significant role. Landman and Luedtke [81] previously showed that the major contribution to the cohesive energy of superlattice originates from van der Waals interactions between passivating molecules from neighbouring nanoparticles. Also Bhattarai et al. [82], who performed MD simulations of Au_{1289} passivated with dodecanothiols, claimed that internal energy decreases with increasing distance between nanoparticles mainly due to van der Waals interaction between alkyl chains. The results which we present here have been obtained in GGA, where van der Waals interactions are severely underestimated. Nevertheless, we still are able to see that the ligand interactions are of more importance for controlling self-assembly of AuNCs rather than interactions between their cores. Their major role can be explained by combination of steric interactions between the bundles of ligands on the facets and related to them changes in electronic properties induced by the vicinity of second NC (see Fig.S3). This result underpins the argument that AuNCs possess unique properties unavailable not only in their bulk limit but also for their larger

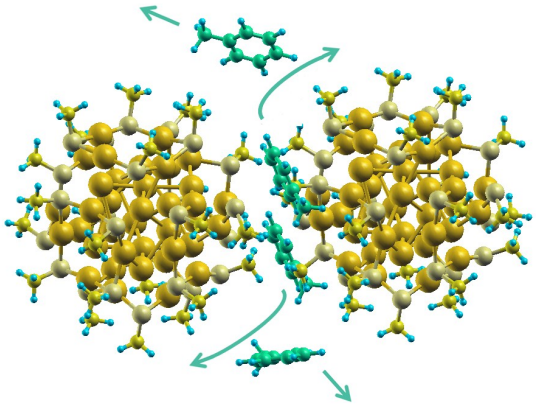

Fig. 6 Visualization of fully optimized system of two $Au_{38}(SCH_3)_{24}$ NCs in the presence of toluene molecules. C atoms in toluene molecules are marked in turquoise color. Green arrows indicate ejection of toluene molecules from the interparticle space. For clarity, eight other toluene molecules present in supercell were removed.

counterparts.

The differences between CST and DFT approaches, as expected, become smaller with increasing size of NC. It appears, the colloidal approach cannot properly describe small NCs due to their non-spherical shape, presence of facets, and unaccounted quantum effects. In effect several basic assumptions in the theory of colloidal interaction break down at this scale[30]. On the other hand, the presented DFT approach does not take into consideration the temperature and pressure effects. Nevertheless, the colloidal approach, especially if the van der Waals interactions of ligands are fully accounted for and the shape of core is taken into consideration, should work well enough to predict interactions between ultra-small nanoparticles.

4 Conclusions

In summary, we have combined two approaches, DFT and CST, in order to evaluate a driving force for the self-assembly of nanoparticles occupying the middle ground between the colloidal and molecular applicability regimes. To this end, we have determined the structural properties and investigated the interaction potentials between AuNCs with different core sizes, symmetry forms, ligand lengths, mutual orientations and in the presence/absence of a solvent. For the first time novel exchange-correlation functionals accounting for van der Waals forces were employed to systems combining metal and organic moieties and consisting of hundreds of atoms. Our calculations demonstrate the dominant role of the ligand-ligand, rather than core-core, interactions in determining the propensity of the AuNCs to form larger assemblies. This is implied by a stronger attractive potential for NCs with longer ligands, in agreement with experimental results, and appears to stem from unusual effects of the bundling of the ligands on the NC facets and related redistribution of electronic charges due to presence of neighbouring NCs. In contrast, CST fails to reproduce this trend, highlighting the need for better understanding of NC interactions governing their assembly for various biomedical and optoelectronic applications.

5 Acknowledgement

This work has been supported by the European Commission through the FP7-NMP programme (project UNION, grant No. 310250). K.Z.M. acknowledges PL-Grid Infrastructure and of Interdisciplinary Centre for Mathematical and Computational Modeling, University of Warsaw (Grant No. G54-8) for providing computer facilities. K.Z.M. also gratefully acknowledges the Gauss Centre for Supercomputing e.V. (www.gauss-centre.eu) for funding this project by providing computing time on Linux Clusters and GCS Supercomputer SuperMUC at Leibniz Supercomputing Centre (project: pr87se). J.K.S. acknowledges funding from the Bavarian State Ministry of Science, Research, and Arts through the grant 'Solar Technologies go Hybrid (SolTech)'.

References

1 M.-C. Daniel and D. Astruc, *Chem. Rev.*, 2004, **104**, 293–346.
2 R. Jin, *Nanoscale*, 2010, **2**, 343–362.
3 A. Fernando, K. L. Dimuthu, M. Weerawardene, N. V. Karimova and C. M. Aikens, *Chem. Rev.*, 2015, **115**, 6112–6216.
4 K. G. Stamplecoskie and P. V. Kamat, *J. Am. Chem. Soc.*, 2014, **136**, 11093–11099.
5 Y. Yu, Z. Luo, D. M. Chevrier, D. T. Leong, P. Zhang, D. Jiang and J. Xie, *J. Am. Chem. Soc.*, 2014, **136**, 1246–1249.
6 W. Zhao, T. Rovere, D. Weerawarne, G. Osterhoudt, N. Kang, P. Joseph, J. Luo, B. Shim, M. Poliks and C.-J. Zhong, *ACS Nano*, 2015, **9**, 6168–6177.
7 A. Corma, P. Concepción, M. Boronat, M. J. Sabater, J. Navas, M. J. Yacaman, E. Larios, A. Posadas, M. A. López-Quintela, D. Buceta, E. Mendoza, G. Guilera and A. Mayoral, *Nature Chemistry*, 2013, **5**, 775–781.
8 E. C. Tyo and S. Vajda, *Nature Nanotech.*, 2015, **10**, 577–588.
9 Z. Wu, J. Liu, Y. Li, Z. Cheng, T. Li, H. Zhang, Z. Lu, and B. Yang, *ACS Nano*, 2015, **9**, 6315–6323.
10 R. L. Whetten, M. N. Shafigullin, J. T. Khoury, T. G. Schaaff, I. Vezmar, M. M. Alvarez and A. Wilkinson, *Acc. Chem. Res.*, 1999, **32**, 397–406.
11 A. K. Boal, F. Ilhan, J. E. DeRouchey, T. Thurn-Albrecht, T. P. Russell and V. M. Rotello, *Nature*, 2000, **404**, 746–748.
12 Z. Nie, A. Petukhova and E. Kumacheva, *Nat. Nanotech.*, 2010, **5**, 15–25.
13 T. M. Carducci and R. W. Murray, *J. Am. Chem. Soc.*, 2013, **135**, 11351–11356.
14 Y. Min, M. Akbulut, K. Kristiansen, Y. Golan and J. Israelachvili, *Nature Mater.*, 2008, **7**, 527–538.
15 K. J. M. Bishop, C. E. Wilmer, S. Soh and B. A. Grzybowski, *Small*, 2009, **5**, 1600–1630.
16 W. D. Luedtke and U. Landman, *J. Phys. Chem.*, 1996, **100**, 13323–13329.
17 T. Geyer, P. Born and T. Kraus, *Phys. Rev. Lett.*, 2012, **109**, 128302.
18 N. Goubet, J. Richardi, P. A. Albouy and M. P. Pileni, *Adv. Func. Mater.*, 2011, **21**, 2693–2704.

19 A. Badia, L. Cucci, L. Demers, F. Morin and R. B. Lennox, *J. Am. Chem. Soc.*, 1997, **119**, 2682–2692.

20 Y. F. Wan, N. Goubet, P. A. Albouy and M. P. Pileni, *Langmuir*, 2013, **29**, 7456–7463.

21 N. Goubet, J. Richardi, P. A. Albouy and M. P. Pileni, *J. Phys. Chem. Lett.*, 2011, **2**, 417–422.

22 N. Schaeffer, Y. Wan and M.-P. Pileni, *Langmuir*, 2014, **30**, 7177–7181.

23 B. Abecassis, F. Testard and O. Spalla, *Phys. Rev. Lett.*, 2008, **100**, 115504.

24 J. B. Smitham, R. Evans and B. Vincent, *J. C. S. Faraday I.*, 1975, **71**, 285.

25 B. Vincent, J. Edwards, S. Emmett and A. Jones, *Colloids and Surfaces*, 1986, **18**, 261.

26 B. A. Korgel, S. Fullam, S. Connolly and D. Fitzmaurice, *J. Phys. Chem. B*, 1998, **102**, 8379–8388.

27 P. Shah, S. Husain, K. P. Johnston and B. A. Korgel, *J. Phys. Chem. B*, 2002, **106**, 12178–12185.

28 T. Sainsbury, J. K. Stolarczyk and D. Fitzmaurice, *J. Phys. Chem. B*, 2005, **109**, 16310–16325.

29 J. K. Stolarczyk, T. Sainsbury and D. Fitzmaurice, *J. Comput.-Aided. Mater. Des.*, 2007, **14**, 151–165.

30 C. A. Batista, R. G. Larson and N. A. Kotov, *Science*, 2015, **350**, 1242477.

31 H. Häkkinen, *Chem. Soc. Rev.*, 2008, **37**, 1847–1859.

32 P. Hohenberg and W. Kohn, *Phys. Rev.*, 1964, **136**, B864–B871.

33 W. Kohn and L. Sham, *Phys. Rev.*, 1965, **140**, 1133–1138.

34 P. Ordejon, E. Artacho and J. M. Soler, *Phys. Rev. B*, 1996, **53**, R10441–R10444.

35 J. M. Soler, E. Artacho, J. D. Gale, A. Garcia, J. Junquera, P. Ordejon and D. Sanchez-Portal, *J. Phys.: Condens. Matter*, 2002, **14**, 2745.

36 J. P. Perdew, K. Burke and M. Ernzerhof, *Phys. Rev. Lett.*, 1996, **77**, 3865–3868.

37 D. M. Ceperley and B. J. Alder, *Phys. Rev. Lett.*, 1980, **45**, 566–569.

38 O. A. Vydrov and T. V. Voorhis, *J. Chem. Phys.*, 2010, **133**, 244103.

39 J. Klimes, D. R. Bowler and A. Michaelides, *J. Phys.: Condens. Matter*, 2010, **22**, 022201.

40 N. Troullier and J. L. Martins, *Phys. Rev. B*, 1991, **43**, 1993.

41 L. Kleinman and D. M. Bylander, *Phys. Rev. Lett.*, 1982, **48**, 1425.

42 H. D. Monkhorst and J. D. Pack, *Phys. Rev. B*, 1976, **13**, 5188.

43 M. Brust, M. Walker, D. Bethell, D. J. Schiffrin and R. Whyman, *J. Chem. Soc., Chem. Commun.*, 1994, 801–802.

44 M. P. Rowe, K. E. Plass, K. Kim, C. Kurdak, E. T. Zellers and A. J. Matzger, *J. Am. Chem. Soc.*, 2004, **16**, 3513–3517.

45 S. Boys and F. Bernardi, *Molecular Physics*, 1970, **19**, 553–566.

46 S. Simon, M. Duran and J. Dannenberga, *J. Chem. Phys.*, 1996, **105**, 11024–11031.

47 K. Z. Milowska and J. A. Majewski, *J. Chem. Phys.*, 2013, **138**, 194704.

48 C. L. Cleveland, U. Landman, T. G. Schaaff, M. N. S. a Peter W. Stephens and R. L. Whetten, *Phys. Rev. Lett.*, 1997, **79**, 1873–1876.

49 R. J. C. Batista, M. S. C. Mazzoni and H. Chacham, *Nanotechnology*, 2010, **21**, 065705.

50 B. S. Gutrath, U. Englert, Y. Wang and U. Simon, *Eur. J. Inorg. Chem.*, 2003, **2013**, 2002–2006.

51 P. D. Jadzinsky, G. Calero, C. J. Ackerson, D. A. Bushnell and R. D. Kornberg, *Science*, 2007, **318**, 430–433.

52 O. Lopez-Acevedo, J. Akola, R. L. Whetten, H. Grönbeck and H. Häkkinen, *J. Phys. Chem. C*, 2009, **113**, 5035–5038.

53 D. Bahena, N. Bhattarai, U. Santiago, A. Tlahuice, A. Ponce, S. B. H. Bach, B. Yoon, R. L. Whetten, U. Landman and M. Jose-Yacaman, *J. Phys. Chem. Lett.*, 2013, **4**, 975–981.

54 D. M. Chevrier, A. Chatt, T. K. Sham and P. Zhang, *J. Phys.: Conf. Series*, 2013, **430**, 012029.

55 M. Azubel, J. Koivisto, S. Malola, D. Bushnell, G. L. Hura, A. L. Koh, H. Tsunoyama, T. Tsukuda, M. Pettersson, H. Häkkinen and R. D. Kornberg, *Science*, 2014, **345**, 909–912.

56 V. G. Yarzhemsky and C. Battocchio, *Russ. J. Inorg. Chem.*, 2011, **56**, 2147–2159.

57 D. Krüger, H. Fuchs, R. Rousseau, D. Marx and M. Parrinello, *J. Chem. Phys.*, 2001, **115**, 6085–6094.

58 N. Goubet and M.-P. Pileni, *Nano Research*, 2014, **7**, 171–179.

59 M. M. Mariscal, J. A. Olmos-Asar, C. Gutierrez-Wing, A. Mayoral and M. J. Yacaman, *Phys. Chem. Chem. Phys.,*, 2010, **12**, 11785–11790.

60 D. Jiang, M. L. Tiago, W. Luo and S. Dai, *J. Am. Chem. Soc.*, 2008, **130**, 2777–2779.

61 H. Häkkinen, M. Walter and H. Grönbeck, *J. Phys. Chem. B*, 2006, **110**, 9927–9931.

62 H. Häkkinen, *Nature Chem.*, 2012, **4**, 443–455.

63 M. A. Boles, D. Ling, T. Hyeon and D. V. Talapin, *Nature Mater.*, 2016, **15**, 141âĂŞ153.

64 R. Cuadrado, J. M. Puerta, F. Soria and J. I. Cerdá, *J. Chem. Phys.*, 2013, **139**, 034319.

65 T. Shimizu, T. Teranishi, S. Hasegawa and M. Miyake, *J. Phys. Chem. B*, 2003, **107**, 2719–2724.

66 H. Hinterwirth, S. Kappel, T. Waitz, T. Prohaska, W. Linder and M. Lämmerhofer, *ACS Nano*, 2013, **7**, 1129–1136.

67 W. W. Weare, S. M. Reed, M. G. Warner and J. E. Hutchison, *J. Am. Chem. Soc.*, 2000, **122**, 12890–12891.

68 H. Qian, M. Zhu, U. N. Andersen and R. Jin, *J. Phys. Chem. A*, 2009, **113**, 4281–4284.

69 S. Mustalahti, P. Myllyperkiö, T. Lahtinen, K. Salorinne, S. Malola, J. Koivisto, H. Häkkinen and M. Pettersson, *J. Phys. Chem. C*, 2014, **118**, 18233–18239.

70 I. G. Shuttleworth, *J. Phys. Chem. Sol.*, 2015, **86**, 19–26.

71 P. Schapotschnikow, R. Pool and T. J. H. Vlugt, *Nano Lett.*, 2008, **8**, 2930–2934.

72 P. Schapotschnikow and T. J. H. Vlugt, *J. Chem. Phys.*, 2009, **131**, 124705.

73 R. Pool, P. Schapotschnikow and T. J. H. Vlugt, *J. Phys. Chem. B*, 2007, **111**, 10201–10212.

74 T. Djebaili, J. Richardi, S. Abel and M. Marchi, *J. Phys. Chem. C*, 2013, **117**, 17791–17800.

75 M. J. Hostetler, J. J. Stoke and R. W. Murray, *Langmuir*, 1996, **12**, 3604–3612.

76 J. E. Martin, J. P. Wilcoxon, J. Odinek and P. Provencio, *J. Phys. Chem. B*, 2000, **104**, 9475–9486.

77 S. J. Khan, F. Pierce, C. M. Sorensen and A. Chakrabarti, *Langmuir*, 2009, **25**, 13861–13868.

78 Y. Wan, H. Portales, N. Goubet, A. Mermet and M.-P. Pileni, *Nano Research*, 2013, **6**, 611–618.

79 J. K. Stolarczyk, A. Deak and D. F. Brougham, *Adv. Mater.*, 2016, 10.1002/adma.201505350.

80 Y. F. Wan, N. Goubet, P. A. Albouy, N. Schaeffer and M. P. Pileni, *Langmuir*, 2013, **29**, 13576–13581.

81 U. Landman and W. D. Luedtke, *J. Phys. Chem.*, 2004, **125**, 1–22.

82 N. Bhattarai, S. Khanal, D. Bahena, J. A. Olmos-Asar, A. Ponce, R. L. Whetten, M. M. Mariscal and M. Jose-Yacaman, *Phys. Chem. Chem. Phys.*, 2014, **16**, 18098–18104.